



Highly efficient activated carbon loaded TiO₂ for photo defluorination of pentafluorobenzoic acid

L. Ravichandran, K. Selvam, M. Swaminathan*

Department of Chemistry, Annamalai University, Annamalai Nagar 608002, India

ARTICLE INFO

Article history:

Received 17 July 2009

Received in revised form 23 October 2009

Accepted 27 October 2009

Available online 5 November 2009

Keywords:

AC-TiO₂

PFBA

Defluorination

Synergistic effect

Photocatalysis

ABSTRACT

The activated carbon loaded TiO₂-P25 catalysts were prepared and characterized by diffuse reflectance spectra (DRS), FT-IR, scanning electron micrograph (SEM), X-ray diffraction (XRD) and BET surface area analysis. The photocatalytic efficiency of activated carbon loaded TiO₂-P25 (AC-TiO₂-P25) was evaluated by UV assisted photodefluorination of pentafluorobenzoic acid (PFBA) in aqueous medium. The catalyst exhibited higher photo defluorination efficiency of PFBA than that of bare TiO₂-P25. The various experimental parameters like concentration of PFBA, addition of oxidants, amount of catalyst and solution pH for efficient defluorination are reported. The higher efficiency of AC-TiO₂-P25 is due to synergy effect of activated carbon.

© 2009 Elsevier B.V. All rights reserved.

1. Introduction

Though titanium dioxide had been widely used for toxic chemical degradation, there are some practical difficulties such as either filtration of fine TiO₂ or fixation of catalyst particles and efficient utilization of UV/solar light. For these reasons many researchers have been working to increase the efficiencies of these processes by modification of its surface. The design of TiO₂ photocatalyst, anchored or embedded onto support materials with large surface areas that could condense diluted substances would be of great significance, not only to avoid the filtration of small photocatalyst particles, but also to obtain higher efficiency [1,2]. Several authors proposed a number of modifications of the photocatalysts by loading them on supporting materials like alumina, zeolite, clay, activated carbon, etc., and by doping with metal ions [3]. Activated carbon has a large specific surface area and a well developed porous structure, resulting in an attractive force toward organic molecules [4–8]. This increases the adsorption capacity of the photocatalyst.

Organofluoro compounds are now being widely used in pharmaceutical, agrochemical, surfactant and polymer industries due to their thermal stability and enhanced lipophilicity [9,10]. These aromatic fluorinated compounds are quite stable and they have no known natural decomposition [11,12]. Some of them have been detected in environmental waters and in animals. Since these com-

pounds are found to have adverse impact on the health of animals and human beings, the removal of these compounds from environmental components becomes essential [11,13,14]. Photocatalytic mineralisation of these compounds produces CO₂, H₂O and fluoride ions. The fluoride ions can be used for the production of CaF₂, which can be used as a raw material for the manufacture of many fluorinated compounds.

Earlier we reported the defluorination of PFBA using TiO₂-P25 [15], ZnO [16] and Fenton's reagent [17]. Though TiO₂-P25 is found to be more efficient than ZnO in the defluorination of PFBA, its efficiency can be further increased by activated carbon loading. Activated carbon support has been reported to give more promising results, which are attributed to the synergistic effect between the AC and the photocatalyst [18]. In the present paper, we report the preparation and characterization of activated carbon loaded TiO₂-P25 catalyst and its photocatalytic activity on the defluorination of PFBA.

2. Experimental

2.1. Materials

Pentafluorobenzoic acid (PFBA) (99% purity) from Aldrich Chemical Company was used without further purification. A gift sample of TiO₂-P25 was obtained from Degussa (Germany). It has the particle size of 30 nm and BET specific surface area of 55 m²/g. AnalaR grade reagents, H₂O₂ (30%, w/w), (NH₄)₂S₂O₈, KBrO₃ (E. Merck), Na₂CO₃, NaCl and FeSO₄·7H₂O were used as received. The activated carbon from SD Fine Chemicals was used as such. The double-

* Corresponding author. Tel.: +91 4144 220572; fax: +91 4144 238080.
E-mail address: chemres50@gmail.com (M. Swaminathan).

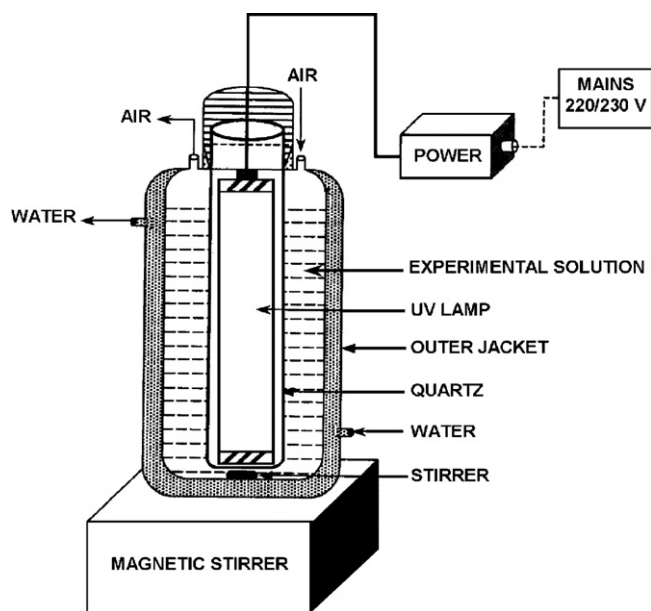


Fig. 1. Schematic diagram of photoreactor.

distilled water was used to prepare experimental solutions. The pH of the solutions was adjusted using H_2SO_4 or NaOH .

2.2. Preparation of AC-TiO₂-P25 catalysts

Catalysts with activated carbon were obtained by mixing TiO₂-P25 and activated carbon at different proportions in water and this aqueous suspension was continuously stirred for 3 h. After this, the mixture was filtered and dried. The catalysts have been denoted as xAC-TiO₂-P25, where 'x' is the weight percentage of activated carbon (w/w) used in the preparation of the catalyst.

Catalysts with the lower AC contents (4%AC-TiO₂-P25 and 8%AC-TiO₂-P25) acquire a clear grey color. However, when the AC concentration in the catalyst is increased above 8%, they become darker. The catalyst with higher AC content (12AC-TiO₂-P25) is practically black.

2.3. Photoreactor

The photocatalytic defluoridation has been carried out with a Heber immersion type photoreactor model HIPR-LP 6/8/116 whose schematic diagram is shown in Fig. 1. This model consisted of a double walled immersion well made of a quartz reactor of 175 cm³ capacity. A small inlet tube is extended down the annular space to ensure flow of the coolant from bottom of well upwards to outlet. In the center of cylindrical reactor, the lamp used for light source was placed inside the quartz tube. For the experiments, lamps with different wavelength emissions were used. One was 16 W low pressure mercury with emission mainly on the mercury resonance line at 253.7 nm. The other was 8 W medium pressure mercury lamp with broadband emission predominantly at 365 nm. For both the lamps photon flux of the light source was determined by ferrioxalate actinometry [19] and the values of 16 W low pressure Hg lamp and 8 W medium pressure Hg lamp are $I_{254\text{ nm}} = 2.54 \times 10^{-5}$ Einstein L⁻¹ s⁻¹, $I_{365\text{ nm}} = 2.08 \times 10^{-6}$ Einstein L⁻¹ s⁻¹ respectively. The reaction vessel had an arm at the top for gas purging. The temperature of the experimental solution was maintained at 25 ± 1 °C by circulating water during the experiments. The above setup was placed in the magnetic stirrer for complete mixing of the catalyst.

2.4. Defluoridation analysis

Fluoride ion concentration was determined using Orion expandable ion analyzer model (EA940). The analysis was done using fluoride ion selective electrode in conjugation with Ag/AgCl reference electrode. The instrument was calibrated using standard sodium fluoride solution of various concentrations between 10 and 250 ppm of fluoride ion. The sample 5 mL from photochemical reactor was taken into 50 mL of polyethylene beaker at a regular interval of 30 min. Five milliliters water and 20 mL total ionic strength adjustable buffer (TISAB) were added to the solution. This solution was stirred for 5 min and fluoride ion concentration was measured. The pH of the solutions was measured using Metrohm 744 pH meter.

2.5. Adsorption experiments

The adsorption experiments have been performed with the PFBA solutions at different concentrations and at different pH. Fifty milliliters aqueous PFBA solution and the catalyst were mixed for 3 h at 25 °C using mechanical shaker. In order to avoid the photoreaction of catalyst, the samples were kept in dark for the entire period of the experiment. After adsorption, the solutions were centrifuged to separate the catalyst. The concentration of the substrate in solution was determined from its absorbances at 270 nm.

2.6. Equipments used

Scanning electron microscopic (SEM) analysis was performed on platinum coated samples using a Jeol apparatus model JSM-5610 LV, equipped with INCA EDX probe for the energy dispersive X-ray microanalysis (EDX). A Varian Cary 5E UV/VIS-NIR spectrophotometer equipped with an integrated sphere was used to record the diffuse reflectance spectra (DRS). The baseline correction was performed using a calibrated reference sample of barium sulfate. The reflectance spectra of the AC-TiO₂-P25 catalysts were analyzed under ambient conditions in the wavelength range of 200–800 nm. The specific surface area of the samples was determined through nitrogen adsorption at 77 K on the basis of BET equation using a Sorptomatic 1990 instrument.

Powder X-ray diffraction patterns of ZnO, AC and AC-ZnO catalysts were obtained using a Philips PANalytical X'per PRO diffractometer equipped with a Cu tube for generating a Cu K α radiation (wavelength 1.5406 Å) at 40 kV, 25 mA. The particles were spread on a glass slide specimen holder and the scattered intensity was measured between 20° and 85° at a scanning rate of $2\theta = 1.2^\circ/\text{min}$ at 25 °C temperature. The digital output of the proportional X-ray detector and the goniometer angle measurements were sent to an online microcomputer for storing and analysis. Peak positions were compared with the standard files to identify the crystalline phases.

For FT-IR experiments, FT-IR spectrophotometer Thermo Nicolet was used. The samples were incorporated in KBr pellets for the measurements. Water reference spectrum was always subtracted from every spectrum. UV spectral measurements were done using Hitachi-U-2001 spectrophotometer. Total organic carbon was mea-

Table 1
Surface area and size of AC-TiO₂-P25 catalysts.

Sample	BET specific surface area (m ² /g)	Crystallite size (nm)
AC	735.60	–
Bare TiO ₂ -P25	55.00	21.5
4AC-TiO ₂ -P25	66.54	27.3
8AC-TiO ₂ -P25	85.60	30.9
10AC-TiO ₂ -P25	92.96	74.8
12AC-TiO ₂ -P25	108.79	74.9

sured with Micro C Model 1997 of Analytica Gena, Germany. HPLC analysis was performed using Shimadzu Prominence Analytical LC model with C-18 Column and UV-detector.

3. Results and discussion

3.1. Characterization

3.1.1. Surface area measurements

The surface area of the catalyst is the most important factor influencing the catalytic activity. Table 1 lists the BET surface area of the TiO₂-P25 and AC-TiO₂-P25 catalysts.

The surface area of the catalyst increases with increase in AC content. A similar trend has been reported in AC-TiO₂ anatase [20]. Higher specific surface area may be of benefit to their high photocatalytic activity due to enhanced absorption of photons and adsorption of pollutants.

3.1.2. Diffuse reflectance spectroscopic analysis

Fig. 2 shows the UV diffuse reflectance spectra of the prepared AC-TiO₂-P25 catalysts along with the bare TiO₂-P25 catalyst. TiO₂-P25 shows a clear absorption edge at around 380 nm with no absorption in visible light region. In AC-TiO₂-P25 samples, absorption of visible light is observed. The visible light absorption increases up to 10AC-TiO₂-P25 and then decreases slightly. It is also noticeable that there is no correlation between the AC content and UV spectrum change. Enhancement of the same order has been observed when the semiconductor has been immobilized on a polymer [21]. It has been reported that the increment of surficial electric charge of oxides such as TiO₂ and WO₃ by the addition of AC gives an absorption increment in the visible and IR region and a color change from white to blue [22]. Similarly catalyst TiO₂-P25 also acquires a color change from white to grey at the lower concentration of AC. This color change may be due to the increment of the electric charge in TiO₂-P25 by the addition of AC. This is produced by the acid base character increment of the surficial hydroxyl groups in the presence of AC. The fact that there is no correlation between the AC content of catalyst and the UV spectrum change reveals that a change of properties in some catalysts is not only determined by their AC content [20].

3.1.3. FT-IR study

In order to understand the surface nature, FT-IR spectra were recorded for the TiO₂-P25 and AC-TiO₂-P25 samples (Fig. 3). FT-

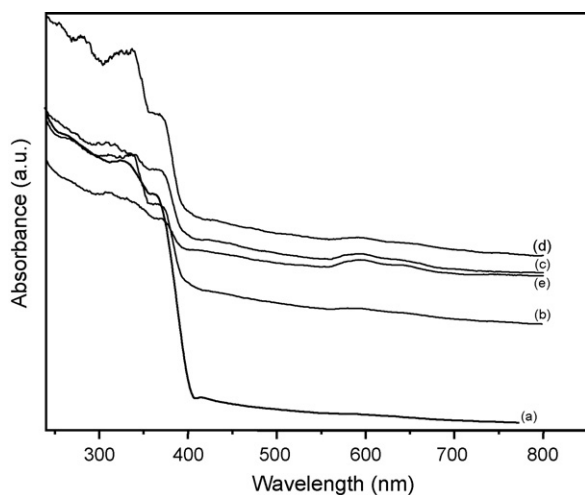


Fig. 2. Diffuse reflectance spectra from the catalysts: (a) bare TiO₂-P25, (b) 4AC-TiO₂-P25, (c) 8AC-TiO₂-P25, (d) 10AC-TiO₂-P25, and (e) 12AC-TiO₂-P25.

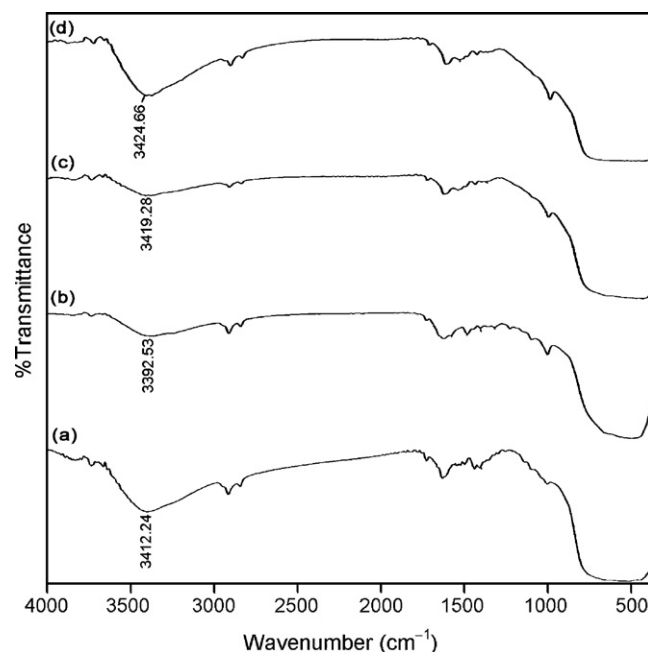


Fig. 3. FT-IR spectra from the catalysts: (a) bare TiO₂-P25, (b) 4AC-TiO₂-P25, (c) 10AC-TiO₂-P25, and (d) 12AC-TiO₂-P25.

IR studies in the region between 4000 and 2500 cm⁻¹ determine possible changes in the distribution of hydroxyl groups that could confirm the above mentioned acid–base character modification of the catalysts. TiO₂-P25 was treated with water as AC-TiO₂ before taking the FT-IR spectrum. In the spectrum of the bare TiO₂-P25 (Fig. 3a) hydroxyl group vibration band is centered at 3412 cm⁻¹. In AC-TiO₂-P25 catalysts a progressive ν_{OH} vibration shift from 3412 to 3424 cm⁻¹ with the increase of AC content of the catalysts is observed (Fig. 3b–d). These vibration shifts have been attributed to an increment of the positive charge of these OH groups [23] adsorbed on the surface of TiO₂-P25, confirming the changes of the acid–base character of the hydroxyl groups in these catalysts.

Furthermore, in the 800–1600 cm⁻¹ region two new bands are obtained. One band corresponding to C–O–C structure is observed at 870–950 cm⁻¹ for AC-TiO₂-P25. The existence of C–O–C structure was reported in investigations of basic activated carbon and also in pyrones which are found to have strong basic sites [24]. The AC-TiO₂-P25, samples show an additional band at the wavelength of 1400–1600 cm⁻¹ which can be attributed to C=C skeleton vibration of aromatic ring. The observation of C–O–C and C=C structure reveals the presence of some basic character in AC-TiO₂-P25.

3.1.4. SEM studies

The texture and morphology the catalyst are very important parameters and might influence the photocatalytic activity. To understand the differences between the TiO₂-P25, activated carbon and AC-TiO₂-P25, SEM images have been analyzed (Fig. 4). The SEM image of AC in Fig. 4a depicts that the crystallinity is more in activated carbon and the surface of the carbon is irregular and not spherical as expected. The SEM image of TiO₂-P25 (Fig. 4b) shows that presence of a porous, sponge like network. It is found that in 10AC-TiO₂-P25 (Fig. 4e) the AC particles are homogeneously covered by TiO₂-P25 particles, which agrees with the previous results [20]. But in 4AC-TiO₂-P25 and 8AC-TiO₂-P25, there is no complete coverage of AC particles by the catalyst (Fig. 4c and d). At higher AC content i.e., 12AC-TiO₂-P25 (Fig. 4f), TiO₂-P25 particles form conglomerates and do not get homogeneously dispersed on AC particles.

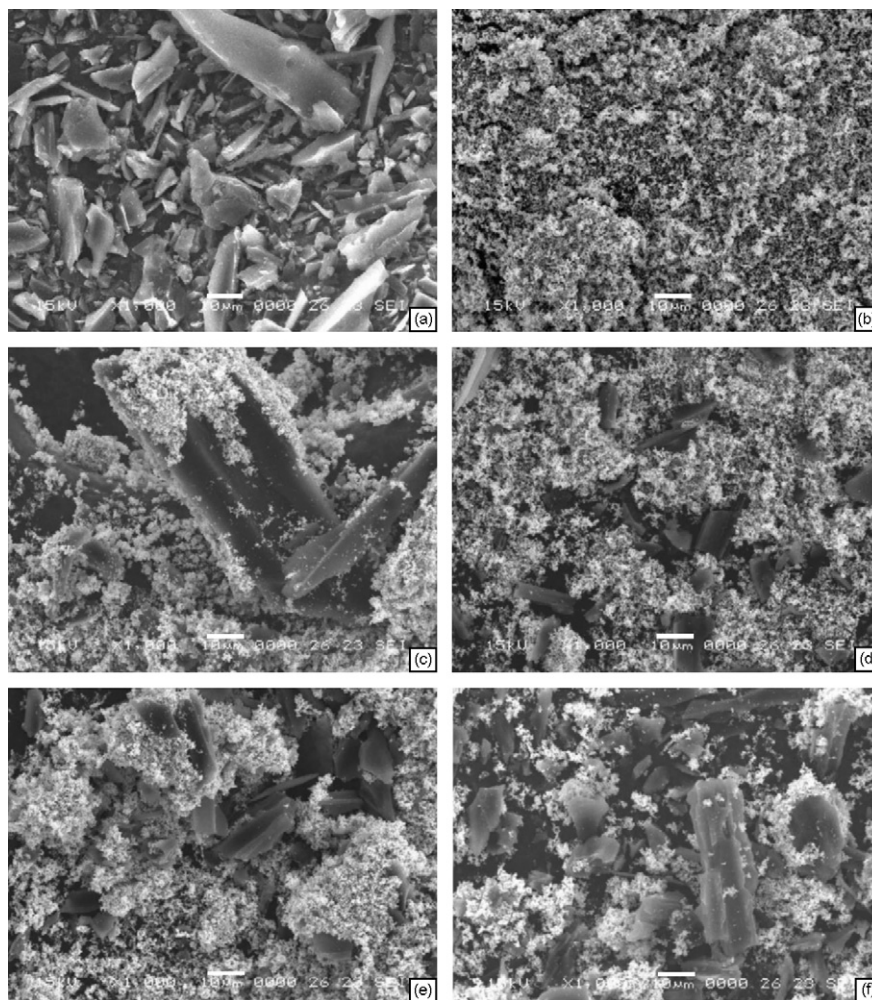


Fig. 4. Scanning electron micrograph images. (a) AC, (b) bare TiO₂-P25, (c) 4AC-TiO₂-P25, (d) 8AC-TiO₂-P25, (e) 10AC-TiO₂-P25, and (f) 12AC-TiO₂-P25 catalysts.

3.1.5. XRD analysis

Fig. 5 shows X-ray diffraction patterns for bare TiO₂-P25, AC and some AC-TiO₂-P25 crystallites with a different content of AC. The X-ray diffraction patterns of AC-TiO₂-P25 almost coincide with that of pure TiO₂-P25 and show no diffraction pattern due to AC, thus suggesting that the AC particles are uniformly distributed on the TiO₂-P25 surface and there is no change in the crystal structure by AC.

The crystal size was determined from the diffraction peak broadening employing the following Eq. (1):

$$D = \frac{K\lambda}{(\beta_c - \beta_s)\cos\theta} \quad (1)$$

where D is the crystal size of the catalyst, λ is the wavelength of X-ray, β_c and β_s are the FWHM of the catalyst and the standard respectively, the value of the coefficient K is 0.89 and θ is the diffraction angle. The sizes of particles are given in Table 1. The crystal size of bare TiO₂-P25 increases from 21.5 nm by the addition of AC.

The results have shown that in the catalysts with AC content lower or equal to 10% in weight TiO₂-P25 particles do not form conglomerates, but get adsorbed on the AC particles surface giving a homogeneous distribution. This regular TiO₂-P25 distribution on AC particles forming layer may be the cause for the charge transference between AC and TiO₂-P25 resulting change in UV–vis absorption spectrum which enhances the catalyst ability to absorb more visible light.

Based on the above results, we have chosen 10AC-TiO₂-P25 for the photocatalytic defluorination of PFBA.

3.2. Photo defluorination

Initially the experiments were carried out to test the photodefluorination of PFBA using 254 nm light with AC-TiO₂-P25 catalysts and the results are shown in Fig. 6. Complete defluorination (180 mg L⁻¹) was observed in 60 min with 10AC-TiO₂-P25 in comparison to 90 min with bare TiO₂-P25. Among the AC-TiO₂-P25 catalysts 10AC-TiO₂-P25 was found to be most efficient. The increased AC content of the catalyst from 4 to 10% increases the fluoride removal. Further increase in AC content to 12%, decreases the fluoride removal efficiency. The enhancement of removal rate is mainly due to the increase in the amount of AC weight which increases the number of PFBA molecules adsorbed. Above 10% of AC in the catalyst, the decrease in removal rate is due to the enhancement of light reflectance by the AC and decrease in light penetration. Thus the optimum amount of AC in the catalyst for efficient photodefluorination of PFBA is 10%.

The defluorination with 10AC-TiO₂-P25 using 254 and 365 nm light was studied to find out the effect of light wavelength and it was compared with the defluorination with bare TiO₂-P25 (Fig. 7). The defluorination is more effective in AC-TiO₂-P25 than bare TiO₂-P25 with both 254 and 365 nm light. The 254 nm (UV-C) light is more efficient than 365 nm (UV-A) light. The morphologies of TiO₂-P25 may be changed with the AC content and the morphology is impor-

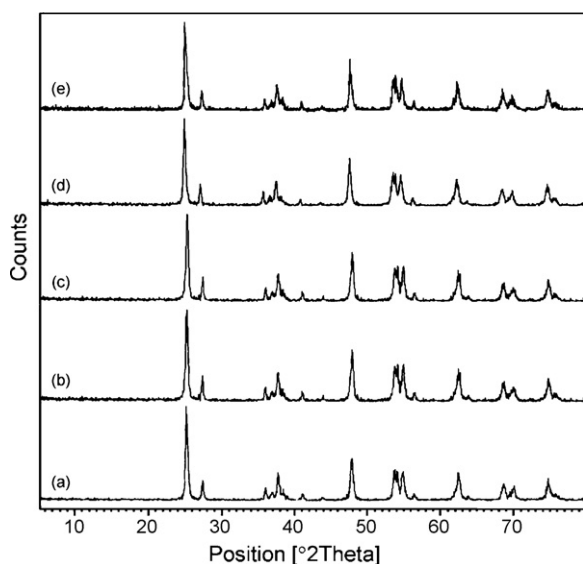


Fig. 5. XRD pattern: (a) bare $\text{TiO}_2\text{-P25}$, (b) 4AC- $\text{TiO}_2\text{-P25}$, (c) 8AC- $\text{TiO}_2\text{-P25}$, (d) 10AC- $\text{TiO}_2\text{-P25}$, and (e) 12AC- $\text{TiO}_2\text{-P25}$.

tant for the photocatalytic activity. To confirm this, the reaction was carried out by the direct addition of activated carbon and $\text{TiO}_2\text{-P25}$ to the reactor with the same concentration of the prepared 10AC- $\text{TiO}_2\text{-P25}$ sample. The defluorination is more effective in prepared AC- $\text{TiO}_2\text{-P25}$ than with direct addition of AC and $\text{TiO}_2\text{-P25}$ separately.

Since the defluorination was effective with 10AC- $\text{TiO}_2\text{-P25}$ using 254 nm light, the effects of pH and oxidants had been carried out using this catalyst and 254 nm light to find out the optimum conditions.

3.2.1. Effect of solution pH

The photocatalytic defluorination efficiency is affected by the surface charge property of the photocatalyst AC- $\text{TiO}_2\text{-P25}$, charge of the molecule, adsorption of molecule onto photocatalyst surface and hydroxyl radical concentration. As these properties are pH dependent, it plays an important role in the degradation of pollutants. The effect of pH from 3 to 11 on the defluorination is shown in Fig. 8.

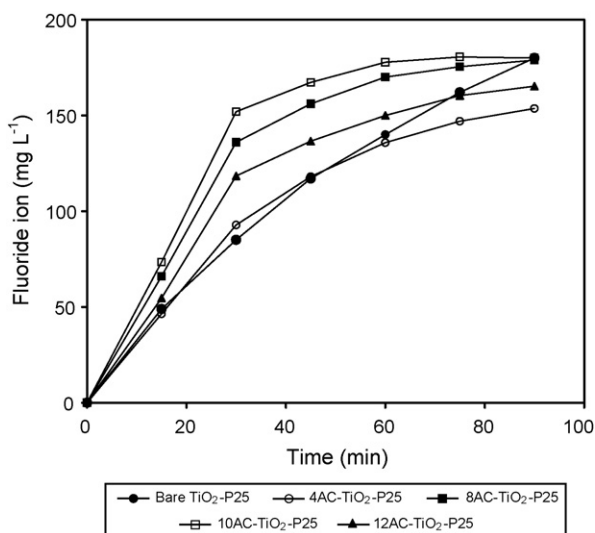


Fig. 6. Primary defluorination of PFBA [PFBA]=400 ppm, catalyst concentration = 1 g/L, pH = 7, airflow rate = 8.1 mL s⁻¹, $I_{254\text{nm}} = 2.54 \times 10^{-5}$ Einstein L⁻¹ s⁻¹.

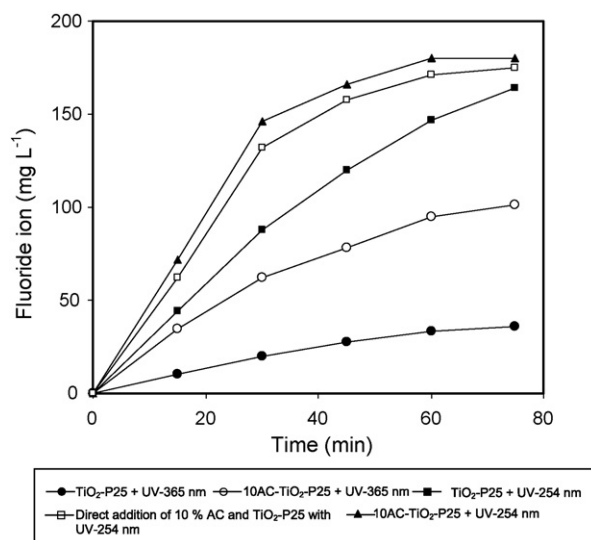


Fig. 7. Comparison of efficiencies of 10AC- $\text{TiO}_2\text{-P25}$ in UV-254 and UV-365 nm light [PFBA]=400 ppm, 10AC- $\text{TiO}_2\text{-P25}$ = 1 g/L, pH = 7, airflow rate = 8.1 mL s⁻¹, $I_{254\text{nm}} = 2.54 \times 10^{-5}$ Einstein L⁻¹ s⁻¹, $I_{365\text{nm}} = 2.08 \times 10^{-6}$ Einstein L⁻¹ s⁻¹.

The pH of the solution is adjusted before irradiation and it is not controlled during the course of the reaction. From the experimental results the photocatalytic defluorination efficiency of AC- $\text{TiO}_2\text{-P25}$ is observed to be higher at neutral pH 7. To find out the reason for this, adsorption experiments were carried out at different pH. The percentages of PFBA remaining after adsorption at different pH are shown in Fig. 9. Maximum adsorption was observed at pH 7. Hence the higher defluorination efficiency is due to the strong adsorption of PFBA on the catalyst surface.

3.2.2. Effect of substrate concentration

The effect of initial PFBA concentration on the defluorination rate was investigated by varying the initial concentration from 100 to 600 mg L⁻¹ at constant pH and catalyst loading. The results are shown in Fig. 10. From the results, it is clear that there is no significant change in defluorination up to 200 ppm while decreasing trend is observed at higher concentrations.

Complete defluorination was observed in 40 min on irradiation of 100 and 200 mg L⁻¹ concentration with 10AC- $\text{TiO}_2\text{-P25}$ in comparison to 90 min with 600 mg L⁻¹. The increase of PFBA concentration decreases the defluorination rate. The rate of deflu-

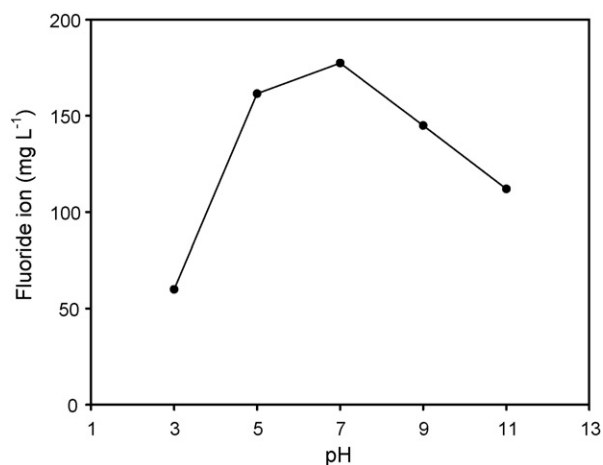


Fig. 8. Effect of pH on photodefluorination of PFBA with 10AC- $\text{TiO}_2\text{-P25}$ [PFBA]=400 ppm, 10AC- $\text{TiO}_2\text{-P25}$ = 1 g/L, airflow rate = 8.1 mL s⁻¹, irradiation time = 60 min, $I_{254\text{nm}} = 2.54 \times 10^{-5}$ Einstein L⁻¹ s⁻¹.

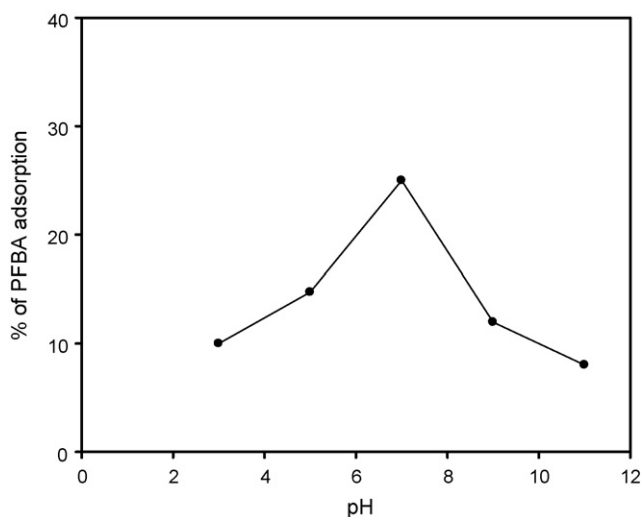


Fig. 9. Effect of adsorption of PFBA with AC-TiO₂-P25 at different pH [PFBA] = 100 ppm, AC-TiO₂-P25 = 100 mg.

oxidation relates the amount of OH radical formation on catalyst surface and the probability of OH radical reacting with PFBA molecules. For all initial PFBA concentrations, the catalyst concentration (175 mg) and UV power (2.54×10^{-5} Einstein L⁻¹ s⁻¹) are same. Since the generation of hydroxyl radical remains constant, the probability of PFBA molecule to react with hydroxyl radical decreases.

Many authors [25] have used the Langmuir–Hinshelwood (L–H) kinetic expression to analyze the heterogeneous photocatalytic reaction. The experimental data have been rationalized in terms of the modified form of L–H kinetic model to describe the solid–liquid reaction successfully [26]. The rate of defluorination of PFBA at the surface is proportional to the surface coverage of PFBA on the catalyst, assuming that the PFBA is strongly adsorbed on the catalyst surface than the intermediate products [26]. The effect of initial PFBA concentration on the initial rate of defluorination is given in

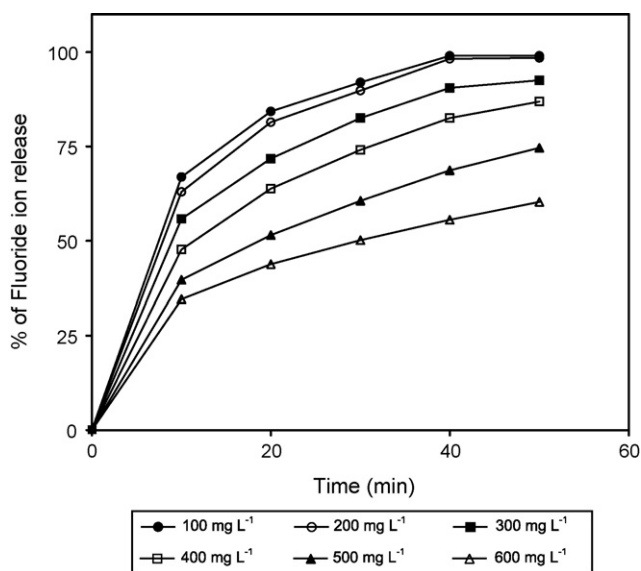


Fig. 10. Effect of initial PFBA concentration on photodefluorination with 10AC-TiO₂-P25. 10AC-TiO₂-P25 = 1 g/L, pH = 7, airflow rate = 8.1 mL s⁻¹, $I_{254\text{nm}} = 2.54 \times 10^{-5}$ Einstein L⁻¹ s⁻¹.

Table 2

Effect of oxidants on photodefluorination of PFBA.

Oxidants	Fluoride ion released (mg L ⁻¹)		
	Without catalyst	With TiO ₂ -P25	With AC-TiO ₂ -P25
KIO ₄	119.6	180	180
H ₂ O ₂	90.1	158.3	90.4
KBrO ₃	80.2	144	172.8
(NH ₄) ₂ S ₂ O ₈	86	146.4	160.2
KClO ₃	18.6	112.5	170.8

[PFBA] = 400 ppm, TiO₂-P25/AC-TiO₂-P25 = 175 mg, oxidants = 125 mg, H₂O₂ = 0.01 M, pH = 7, airflow rate = 8.1 mL s⁻¹, irradiation time = 30 min, $I_{254\text{nm}} = 2.54 \times 10^{-5}$ Einstein L⁻¹ s⁻¹.

the following equation [27]:

$$r = \frac{kKC}{1 + KC} \quad (2)$$

This equation can be modified as:

$$\frac{1}{r} = \frac{1}{kKC} + \frac{1}{k} \quad (3)$$

where C is the initial concentration of PFBA, k is the reaction rate constant and K is the Langmuir adsorption constant. The k reflects the limiting rate of the reaction at maximum coverage under the given experimental conditions and K represents the equilibrium constant for adsorption of PFBA on the illuminated catalyst.

The applicability of L–H equation for adsorption has been confirmed by the linearity of the plot of $1/r$ vs $1/C$. This also indicates that the defluorination of PFBA occurred mainly on the surface of catalyst. The values of k and K determined from the plot are found to be 0.538×10^{-4} M⁻¹ s⁻¹ and 0.300×10^{-4} M⁻¹, respectively for AC-TiO₂-P25.

3.2.3. Effect of inorganic oxidants

Table 2 gives the comparison of defluorination by oxidants, oxidants with catalysts TiO₂-P25 and AC-TiO₂-P25. It can be observed from the table that defluorination is enhanced by the addition of oxidants except H₂O₂. The defluorination efficiency is in the following order: UV/AC-TiO₂-P25/oxidants > UV/TiO₂-P25/oxidants > UV/oxidants.

The enhancement in UV/AC-TiO₂-P25 and UV/TiO₂-P25 by the addition of oxidant is due to increased charge separation caused by oxidants. In case of H₂O₂ the decrease in defluorination is observed. The negative effect of H₂O₂ on some semiconductor photocatalysis of organic compounds had been reported by several authors [28–30]. H₂O₂ may be adsorbed on AC-TiO₂-P25, reducing the activity of the catalyst.

3.3. Synergistic effect

Enhanced photocatalytic activity of semiconductors has been achieved by the processes such as metal doping, surface modification and mixing of two semiconductors, etc. But here we observed the enhanced photocatalytic activity of TiO₂-P25 when loaded with activated carbon. Activated carbon has no photocatalytic activity but it increases the photocatalytic activity of TiO₂-P25 and this is due to the increased adsorption of PFBA on AC-TiO₂-P25. Increased adsorption leads to higher concentration of PFBA around TiO₂-P25. This exhibits synergism, in which the adsorbed PFBA on AC is transferred to TiO₂-P25. The complete degradation of PFBA adsorbed on AC-TiO₂-P25 was confirmed by FT-IR studies. The FT-IR spectra of AC-TiO₂-P25 photocatalyst after the adsorption of PFBA in dark and after complete defluorination on irradiation along with FT-IR spectrum of catalyst alone are shown in Fig. 11a–c. New absorption bands such as 1650, 1613, 1527, 1490, 1402 and 1290 cm⁻¹ appeared on the absorption spectra of the catalyst after PFBA

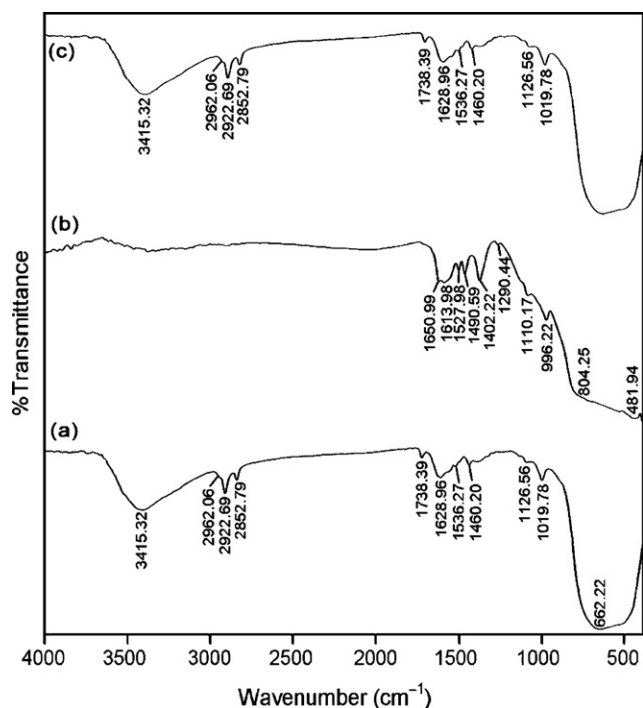
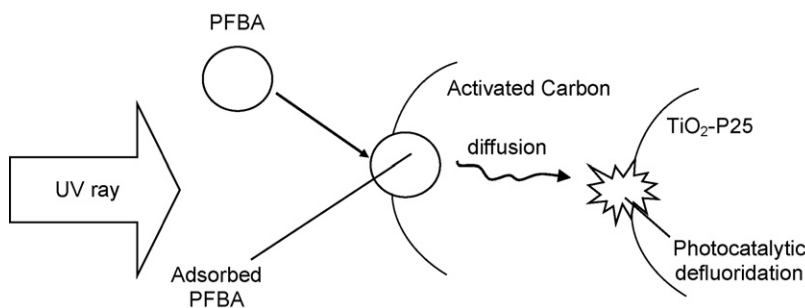


Fig. 11. FT-IR spectra of (a) fresh AC-TiO₂-P25, (b) AC-TiO₂-P25 after PFBA adsorption and (c) AC-TiO₂-P25 after complete defluoridation of PFBA.

adsorption can be assigned to the C–F stretching modes of PFBA on to the catalyst surface (Fig. 11b). In general, fluorine containing compounds exhibit strong absorptions in the region from 1400 to 1000 cm⁻¹ due to C–F stretching modes. After irradiation of AC-TiO₂-P25 with the adsorbed PFBA, peaks in this range disappeared giving a spectrum (Fig. 11c) similar to the spectrum of the catalyst alone (Fig. 11a). This confirms that the adsorbed PFBA molecules on AC are being transferred to the TiO₂-P25, where they are degraded under irradiation as shown in Scheme 1.

3.4. Mineralisation of PFBA

In addition to measurement of defluoridation by fluoride ion selective electrode, it is necessary to confirm the mineralisation by other techniques also. Hence, the irradiated samples of PFBA were analyzed by total organic carbon (TOC) measurement and by HPLC. TOC values for the PFBA irradiated sample (400 ppm initial concentration of PFBA) in UV/AC-TiO₂-P25 catalyst at specified intervals of time are given in Table 3. The value of 10.3 ppm at 90 min indicates 94% degradation, which is very close to complete mineralisation. For observing the trend of degradation, HPLC analysis was done for these samples and the percentages of PFBA are also given in Table 3.



Scheme 1. Synergistic effect of AC-TiO₂-P25 on photodefluoridation of PFBA.

Table 3
TOC and HPLC values of PFBA degradation.

Time (min)	Total organic carbon (ppm)	HPLC analysis (%)
Standard	157	99.4
30	98	68.63
60	54	37.45
90	10.3	6.96

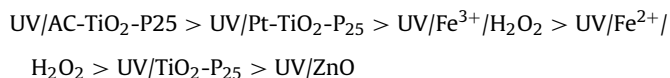
Table 4
Percentages of PFBA defluoridation by various processes (irradiation time = 60 min).

Process	% of defluoridation
UV/TiO ₂ -P25	78.0
UV/ZnO	68.6
UV/Fe ³⁺ /H ₂ O ₂	92.6
UV/Fe ²⁺ /H ₂ O ₂	79.2
UV/AC-TiO ₂ -P25	99.3
UV/Pt-TiO ₂ -P25	97.0

In HPLC, the standard peak for PFBA with retention time of 6 min decreased from 99.45% to 68.63 and 6.96% at the time of 30 and 90 min irradiation respectively. This again confirms about 93% of PFBA degradation in 90 min. Analysis of HPLC after 30 min of irradiation reveals the formation of three peaks with retention times 4.38, 3.68 and 2.81. By matching with the standards, these three peaks are found to be due to the formation of pentafluorobenzene, pentafluorophenol and tetrafluoroquinone as intermediates during the irradiation. The formation of these intermediates in the defluoridation of PFBA by UV-TiO₂-P25 process was already confirmed by GC-MS analysis [15].

3.5. Comparison of photodefluoridation of PFBA

The percentages of photodefluoridation of 400 ppm PFBA with this catalyst is compared to our earlier results reported for the defluoridation of PFBA using the catalysts TiO₂-P25 [15], ZnO [16], Fenton [17] and Pt-TiO₂-P25 [31] at their respective optimum conditions. The results are given in Table 4. Among these catalysts, AC-TiO₂-P25 is found to be most efficient. The order of defluoridation efficiency is as follows:



The advantage of AC-TiO₂-P25 process is that the maximum defluoridation efficiency (99.3%) is observed at neutral pH 7 which is beneficial and easy to implement in any wastewater treatment. Also separation of catalyst becomes easier. The increased efficiency of UV/AC-TiO₂-P25 process can be attributed mainly to the synergism of activated carbon. Moreover light absorption increases due to increment of the surfacial electron charge of the hydroxyl groups in the presence of AC.

4. Conclusions

The increase in the photocatalytic activity of TiO₂-P25 by the addition of activated carbon was observed. Activated carbon was loaded into TiO₂-P25 in 4, 8, 10 and 12% by weight. These catalysts were characterized by various surface analytical methods such as BET surface area measurement, diffuse reflectance spectroscopy, FT-IR spectroscopy, scanning electron microscopy and X-ray diffraction analysis. Among AC-TiO₂-P25 catalysts, 10AC-TiO₂-P25 was found to be most efficient.

The experiments revealed that the defluoridation is more effective in 10AC-TiO₂-P25 than bare TiO₂-P25 and 254 nm is more effective than 365 nm. Complete defluoridation was observed in 60 min with 10AC-TiO₂-P25 in comparison to 90 min with bare TiO₂-P25. The higher photocatalytic defluoridation efficiency of 10AC-TiO₂-P25 at neutral pH is due to synergistic effect of AC. As experienced with other catalysts, increase of PFBA concentration decreases the defluoridation rate. The addition of inorganic oxidants to catalyst enhances the defluoridation efficiency and is in the following order: UV/AC-TiO₂-P25/oxidants > UV/TiO₂-P25/oxidants > UV/oxidants.

Acknowledgements

One of the authors, K. Selvam is thankful to CSIR, New Delhi, for the award of Senior Research Fellowship. We thank Catalysis Laboratory, IIT Madras, Chennai for BET measurements.

References

- [1] S. Sakthivel, S.U. Geissen, D.W. Bahnemann, V. Murugesan, A. Vogelpohl, J. Photochem. Photobiol. A: Chem. 148 (2002) 283–293.
- [2] A. Dipaola, E. Garcia-Lopez, S. Ikeda, G. Marci, B. Ohtani, L. Palmisano, Catal. Today 75 (2002) 87–93.
- [3] R.L. Pozzo, M.A. Baltanas, A.E. Cassano, Catal. Today 39 (1997) 219–231.
- [4] T. Tsumura, N. Kojitani, I. Izumi, N. Iwashita, M. Toyoda, M. Inagaki, J. Mater. Chem. 12 (2003) 1391–1396.
- [5] Y. Xu, W. Zheng, W. Liu, J. Photochem. Photobiol. A: Chem. 122 (1999) 57–60.
- [6] K. Shimizu, T. Kaneko, T. Fujishima, T. Kodama, H. Yosida, Y. Kitayama, Appl. Catal. A: Gen. 225 (2002) 185–191.
- [7] J. Matos, J. Laine, J.M. Herrmann, J. Catal. 200 (2001) 10–20.
- [8] J. Arana, J.M. Dona Rodriguez, C. Garriga i Cabo, O. Gonzalez-Diaz, J.A. Herrera-Melian, J. Perez Pena, G. Colon, J.A. Navio, Appl. Catal. B: Environ. 44 (2003) 161–172.
- [9] S.J. Tavener, J.H. Clark, J. Fluorine Chem. 123 (2003) 31–36.
- [10] R. Natarajan, R. Azerad, B. Badet, E. Copin, J. Fluorine Chem. 126 (2005) 424–435.
- [11] R. Renner, Environ. Sci. Technol. 35 (2001) 154A.
- [12] J.P. Giesy, K. Kannan, Environ. Sci. Technol. 36 (2002) 146A–152A.
- [13] K.J. Hansen, H.O. Johnson, J.S. Eldridge, J.L. Buehner, L.A. Dick, Environ. Sci. Technol. 36 (2002) 1681–1685.
- [14] K. Kannan, J.W. Choi, N. Iseki, K. Senthilkumar, D.H. Kim, S. Masunaga, G.P. Giesy, Chemosphere 49 (2002) 225–231.
- [15] L. Ravichandran, K. Selvam, M. Muruganandham, M. Swaminathan, J. Fluorine Chem. 127 (2006) 1204–1210.
- [16] L. Ravichandran, K. Selvam, M. Swaminathan, Sep. Purif. Technol. 56 (2007) 192–198.
- [17] L. Ravichandran, K. Selvam, M. Swaminathan, J. Photochem. Photobiol. A: Chem. 188 (2007) 392–398.
- [18] E. Carpio, P. Zuniga, S. Ponce, J. Solis, J. Rodriguez, W. Estrada, J. Mol. Catal. A 228 (2005) 293–298.
- [19] C.G. Hatchard, C.A. Parker, Proc. R. Soc. London A 235 (1956) 518.
- [20] J. Arana, J.M. Dona-Rodriguez, E. Tello-Rendon, C. Garriga-i-Cabo, O. Gonzalez-Diaz, J.A. Herrera-Melian, J. Perez-Pena, G. Colon, J.A. Navio, Appl. Catal. B 44 (2003) 153–160.
- [21] V. Brezova, M. Jankovicova, M. Soldan, A. Blazkova, M. Rehakova, I. Surina, M. Ceppan, B. Havilinova, J. Photochem. Photobiol. A 89 (1994) 69–75.
- [22] I. Bedja, S. Hotchandani, P.V. Kamat, J. Phys. Chem. 97 (1993) 11064–11070.
- [23] P.A. Connor, K.D. Dobson, A.J. McQuillan, Langmuir 15 (1999) 2402–2408.
- [24] E. Papirer, S. Li, J.B. Donnet, Carbon 25 (1987) 243–247.
- [25] L. Wenhua, L. Hong, C. Sao'an, Z. Jianqing, C. Chunan, J. Photochem. Photobiol. A 131 (2000) 125–132.
- [26] H. Al-Ekabi, N. Serpone, J. Phys. Chem. 92 (1988) 5726–5731.
- [27] R.W. Matthews, J. Phys. Chem. 91 (1987) 3328–3333.
- [28] J. Harbour, J. Tromp, M.L. Hair, Can. J. Chem. 63 (1985) 204–208.
- [29] C. Kormann, D.W. Bahnemann, M.R. Hoffmann, Environ. Sci. Technol. 22 (1988) 798–806.
- [30] E. Evgenidou, K. Fytianos, I. Poullos, Appl. Catal. B 59 (2005) 81–89.
- [31] L. Ravichandran, K. Selvam, B. Krishnakumar, M. Swaminathan, J. Hazard. Mater. 167 (2009) 763–769.